Partially Folded States of Staphylococcal Nuclease Highlight the Conserved Structural Hierarchy of OB-Fold Proteins †

ARTICLE *in* BIOCHEMISTRY · SEPTEMBER 2007

Impact Factor: 3.02 · DOI: 10.1021/bi700532j · Source: PubMed

4 AUTHORS, INCLUDING:

Emma Watson
Harvard Medical School
7 PUBLICATIONS **138** CITATIONS
SEE PROFILE

Andrei T Alexandrescu
University of Connecticut
74 PUBLICATIONS **2,215** CITATIONS
SEE PROFILE

Published in final edited form as:
Biochemistry. 2007 August 21; 46(33): 9484–9494.

Partially Folded States of Staphylococcal Nuclease Highlight the Conserved Structural Hierarchy of OB-Fold Proteins†

Emma Watson‡, **William M. Matousek**‡, **Evelyn L. Irimies**, and **Andrei T. Alexandrescu***
Department of Molecular and Cell Biology, University of Connecticut, Storrs, Connecticut 06269

Abstract

We have been interested in whether three proteins that share a five-stranded *β*-barrel "OB-fold" structural motif but no detectable sequence homology fold by similar mechanisms. Here we describe native-state hydrogen exchange experiments as a function of urea for SN (staphylococcal nuclease), a protein with an OB-fold motif and additional nonconserved elements of structure. The regions of structure with the largest stability and unfolding cooperativity are contained within the conserved OB-fold portion of SN, consistent with previous results for CspA (cold shock protein A) and LysN (anticodon binding domain of lysyl tRNA synthetase). The OB-fold also has the subset of residues with the slowest unfolding rates in the three proteins, as determined by hydrogen exchange experiments in the EX1 limit. Although the protein folding hierarchy is maintained at the level of supersecondary structure, it is not evident for individual residues as might be expected if folding depended on obligatory nucleation sites. Rather, the site-specific stability profiles appear to be linked to sequence hydrophobicity and to the density of long-range contacts at each site in the three-dimensional structures of the proteins. We discuss the implications of the correlation between stability to unfolding and conservation of structure for mechanisms of protein structure evolution.

The concept of a protein fold as a recurrent unit of structure is central to modern structural biology. One of the goals of The Protein Structure Initiative is to determine representative examples of all folds (1), estimated to number between 1000 (2) and 10 000 (1,3,4). The difficulty of protein structure prediction targets and the approaches for modeling unknown structures are often predicated on whether the protein is likely to have a novel fold (5). Inferences about evolutionary relationships are often made on the basis of protein folds, because structure can be conserved even when sequences have diverged to levels where sequence homology is no longer detectable (6). While the concept of a protein fold is generally accepted, the classification of folds in practice remains somewhat subjective and ambiguous.

The OB-fold[1] (Figure 1) was originally described as an oligonucleotide/oligosaccharide-binding fold (7) and consists of a five-stranded *β*-barrel structure. It is represented well in both sequence and structure databases (3,8–10). The October 2006 release of the SCOP database (11) classifies some 95 protein domains as OB-fold structures. These are grouped into 27 function families with activities ranging from molybdate-binding proteins to RNA chaperones.

---

†This work was supported by NSF Grant MB 0236316 to A.T.A., a Richard Crain Jr. Memorial Fellowship to W.M.M., and a Todd M. Schuster undergraduate summer fellowship to E.W.

* To whom correspondence should be addressed: Department of Molecular and Cell Biology, University of Connecticut, 91 N,. Eagleville Rd., U-3125, Storrs, CT 06269–3125., Telephone: (860) 486–4414., Fax: (860) 486–4331., E-mail: andrei@uconn.edu..
‡These authors contributed equally to this work.

[1]Abbreviations: CspA, cold shock protein A; k_{obs}, observed hydrogen exchange rate; k_{int}, intrinsic hydrogen exchange rate; ΔG_{HX}, free energy change for hydrogen exchange; ΔG_{fluct}, denaturant-independent contribution to ΔG_{HX} from noncooperative structure fluctuations; ΔG_{unf}, denaturant-dependent contribution to ΔG_{HX} from cooperative partial or global unfolding of the structure; HSQC, heteronuclear single-quantum correlation; HX, hydrogen exchange; LysN, N-terminal anticodon binding domain of lysyl tRNA synthetase; *m*, slope of the denaturant concentration dependence of ΔG; NSHX, native-state hydrogen exchange; OB-fold, oligonucleotide/oligosaccharide-binding fold composed of a five-stranded antiparallel Greek key β-barrel; SN, staphylococcal nuclease; SNOB, folded fragment of residues 1–103 of SN with the global suppressor mutations V66L and G88V.

These families are further grouped into 10 superfamilies that are hypothesized to have a common evolutionary origin (11).

Representative structures classified as OB-fold domains in the SCOP database are shown in Figure 1A. The secondary structures range from 3 to 10 strands of β-sheet. Many of these proteins have additional α-helices that are not conserved. It has been duly noted that structure similarity spans a continuum, much like sequence similarity (3). As such, the classification of protein structures according to discrete "folds" may be somewhat artificial, particularly if the point of the classification is to infer functional relationships. Another motivation for the classification of proteins into fold families is to discern evolutionary relationships (1). Here, care must be exercised to distinguish convergent from divergent evolution (12). Structures related through divergent evolution are derived from a shared immediate ancestor, whereas in convergent evolution, similar structural features arise independently to satisfy a functional role. Our working hypothesis is that information about protein folding can help distinguish evolutionary relationships among structures, much in the same way that protein structures can reveal homology not apparent from a comparison of protein sequences. To this end, our lab has carried out comparative folding studies of three proteins from the nucleotide-binding branch of the OB-fold family (Figure 1B): CspA (cold shock protein A), LysN (anticodon binding domain of lysyl tRNA synthetase), and SN (staphylococcal nuclease). CspA is a mRNA chaperone that binds mRNA in such a way that it facilitates translation when *Escherichia coli* are grown at low temperatures (13). LysN recognizes the anticodon loop of lysyl tRNA (14). SN is a phosphodiesterase secreted by *Staphylococcus aureus* that hydrolyzes DNA or RNA to 3′-mononucleotides in the presence of Ca^{2+} (15). The three proteins bind oligonucleotides roughly on the same location of their β-barrels, with most of the polar residues involved in substrate binding coming from loops L_{12}, L_{34}, and L_{45} (7). The conservation of structure and ligand recognition motifs makes the OB-fold an excellent model system for determining if similarity also extends to folding mechanisms. We initially looked at the proteins using mutagenesis and found that the OB-fold has the properties of an independent folding module (16, 17). To obtain more complete information, we extended our comparative studies to the native-state hydrogen exchange (NSHX) method (18, 19).

Hydrogen exchange (HX) is a powerful tool for studying the stabilities and dynamics of proteins. Exposed amide protons exchange with solvent according to intrinsic rates that can be calculated from the solution pH, temperature, and amino acid sequence (20,21). Exchange can be slowed by structure, and the ratio of observed to intrinsic rates gives site-specific information about the stability of structure (20). Protected amide protons can exchange by two mechanisms: localized noncooperative breathing motions or unfolding of part or the entire structure. The mechanisms can be distinguished from the denaturant dependence of HX, which forms the basis of the NSHX method (19,20). Localized breathing motions expose little new surface area to solvent and are independent of denaturant concentration. By contrast, cooperative partial or complete unfolding of the protein exposes a large new surface area to solvent, and plots of exchange rates versus denaturant concentration have non-zero slopes (m_{HX} values). The NSHX experiments are conducted over a range of denaturant concentrations where the native state always predominates (>99% N state). Exchange occurs through transiently formed high-energy states that become more populated as the denaturant concentration increases (20,22). The dependence of the data on denaturant concentration provides information about the stability of the native structure in the absence of denaturant (ΔG^{o}_{unf}) and about the cooperativity of unfolding (m_{HX}).

We previously used the NSHX experiment to characterize the free energy landscape of CspA and LysN. Here we bring these studies to completion with an investigation of SN. The results show that the structurally conserved β-barrel portion of the structure is more stable to unfolding and more cooperatively stabilized than the nonconserved elements of structure. The hierarchy

of structural stability in SN is similar to that previously defined for LysN and CspA. In addition to the NSHX experiments, we obtained data at pH 10.2 where exchange is in the EX1 limit and determined the rates with which "open" exchange-susceptible conformations are generated for the subset of slowest exchanging amide protons (22,23). These experiments indicate that the structurally conserved OB-fold core, which has the greatest stability to unfolding, also has the slowest unfolding rates.

EXPERIMENTAL PROCEDURES

Materials

SN with the wild-type sequence of the *S. aureus* Foggi strain was expressed in *E. coli* JM109 (DE3) cells containing plasmid *pSNWT11a* (24), a gift from J. Flanagan (The Pennsylvania State University, State College, PA). Cells were grown at 28 °C in MOPS minimal medium (25) supplemented with 1 g/L $^{15}NH_4Cl$ to an OD_{600} of ~0.6 and induced to produce SN by adding 0.57 mM IPTG. The culture was incubated at 30 °C with shaking at 150 rpm for an additional 4 h. Protein was purified using urea extraction, ethanol precipitation, and SP-Sepharose fast flow ion exchange chromatography (Amersham) as previously described (26, 27). Samples for NMR were verified to be >90% pure by SDS–PAGE, dialyzed one time against 1 M NaCl and three times against milli-Q water, freeze-dried, and stored at −20 °C prior to use. SN concentrations were determined using an extinction coefficient $A_{280,1\ mg/mL}$ of 0.93 (28). ^{15}N-labeled CspA (29,30) and LysN (14,16) for HX experiments at high pH were obtained using previously published protocols. All three proteins gave $^{1}H–^{15}N$ HSQC spectra indistinguishable from those previously published, attesting to the purity of the samples. $^{1}H–^{15}N$ HSQC resonances from all three proteins were assigned on the basis of published spectra (14,31–34). Urea (ultra analytical grade) was from Sigma (St. Louis, MO), and sodium acetate trihydrate was from J. T. Baker (Phillipsburg, NJ).

Native-State Hydrogen Exchange Experiments for SN

NMR data were collected on a Varian Inova instrument operating at 600 MHz. Samples for the NSHX experiments had SN concentrations of 10 mg/mL (0.60 mM), in a 99.96% D_2O buffer of 20 mM sodium acetate. Data were collected at nine urea concentrations (0, 0.14, 0.24, 0.32, 0.43, 0.62, 0.83, 1.09, and 1.26 M). Urea concentrations were determined by refractometry (35). The pH values for the nine experiments ranged between pH 5.3 and 5.8, and intrinsic rates were calculated accordingly using SPHERE (21). Exchange was monitored with two-dimensional sensitivity-enhanced gradient $^{1}H–^{15}N$ HSQC experiments (36) acquired with 1024 ^{1}H × 64 ^{15}N complex points and spectral widths of 8000 Hz × 2180 Hz. Between 18 and 41 time points were collected for each urea concentration with total experiment times ranging from ~2 h at high urea concentrations to ~5 days at low urea concentrations.

A total of 64 of the protein's 142 non-proline residues were used to characterize amide proton exchange. Analyses of the HX data were conducted using custom FELIX macros that quantify peak intensities as a function of time in D_2O. Exchange data for each residue were fit to a single-exponential decay to a baseline value:

$$I = I_0 \exp(-k_{obs} t) + C \quad (1)$$

where I_0 is the initial peak intensity, k_{obs} is the observed HX rate, and C is the baseline noise of the spectrum. The fits were done with KaleidaGraph version 3.6 (Synergy Software).

HX experiments between pH 5.3 and 7.0 were used to verify (23,37,38) that exchange was in the EX2 limit under the conditions of the NSHX experiments for SN. The free energy difference

between exchange-resistant “closed” conformations and exchange-susceptible “open” conformations that allow exchange was calculated as

$$\Delta G_{HX} = -RT \ln (K_{ex}) = -RT \ln ([open]/[closed]) = -RT \ln (k_{obs}/k_{int}) \quad (2)$$

where k_{obs} is the observed HX rate constant and k_{int} is the intrinsic HX rate constant (16,19, 22,38) estimated with SPHERE (21). Uncertainties for k_{obs} values were taken as the standard errors of the fits to eq 1 and were propagated for the ΔG_{HX} values as previously described (16).

The free energy difference for exchange, ΔG_{HX}, can have contributions from local breathing reactions (ΔG_{fluct}), which are independent of denaturant concentration, and contributions from unfolding reactions (ΔG_{unf}), which become favored with increasing denaturant concentrations (18,19,39). The model in which both these mechanisms contribute is given by (19)

$$\Delta G_{HX} = -RT \ln \left(\exp \frac{-\Delta G_{fluct}}{RT} + \exp \frac{m_{HX}[urea] - \Delta G^{o}_{unf}}{RT} \right) \quad (3)$$

where m_{HX} is the slope of the urea concentration dependence of ΔG_{HX}. In many cases, ΔG_{fluct} makes no contribution (38) and the data obey a simple model in which ΔG_{HX} depends linearly on denaturant concentration:

$$\Delta G_{HX} = \Delta G^{o}_{unf} - m_{HX}[urea] \quad (4)$$

The model of eq 3 contains three adjustable parameters (m_{HX}, ΔG^{o}_{unf}, and ΔG_{fluct}), while that of eq 4 contains two adjustable parameters (m_{HX} and ΔG^{o}_{unf}). The F-test on the limiting ratio of the reduced sum of squared errors (40) was used to establish if the data warranted being fit to the more complicated model (eq 3).

Hydrogen Exchange at Basic pH

The fastest exchanging protons were identified from correlations in FAST-HSQC spectra (41) that were lost going from pH 7 to 11. To establish that exchange was in the EX1 limit for the subset of the slowest exchanging amide protons that survived at pH 10.2 in D_2O, we collected 1H-^{2}H isotope exchange data at pH 6.0, 7.0, 8.1, 9.3, 9.9, and 10.6 for LysN and at pH 5.3, 7.0, 8.5, and 10.2 for SN. The EX1 limit was inferred from the plateau in the HX rates reached at basic pH (23).

RESULTS

Native-state hydrogen exchange of SN was monitored at urea concentrations ranging from 0 to 1.2 M. Figure 2 shows representative time points for the experiment without urea. Exchange for SN is relatively fast (31,32,42), and under the conditions of this study (pH 5.3 and 25 °C), nearly all amide protons exchanged within 5 days. Peaks that survived longer than 1 h in D_2O were for the most part involved in hydrogen-bonded secondary structure. Notable exceptions include the segment of residues 97–101 that is strongly protected by irregular structure and solvent exclusion. After 10 h in D_2O, all the signals from C-terminal helix α2 were gone (violet). Most of the signals left after 16 h were from amide protons in the OB-fold motif (cyan, red, and green).

Exchange rates increased with urea concentration as illustrated for the representative residue Lys24 in Figure 3. ΔG_{HX} values were calculated from the experimental and intrinsic exchange

rates according to eq 2 (16,19–22). Nearly all residues exhibited a linear dependence of ΔG_{HX} on denaturant concentration (Figure 4). This type of linear dependence is typical of exchange through a cooperative partial or complete unfolding of the protein (16,18,19,38), where the slope (m_{HX}) is proportional to the increase in solvent accessible area that accompanies unfolding (19,22,43). An alternative mechanism involving noncooperative localized fluctuations of the structure predicts an initially negligible dependence of ΔG_{HX} on denaturant concentration, followed by a steep dependence as unfolding becomes increasingly promoted (18,19,39). Of the 64 residues that were examined, an F-test (40) indicated that the use of the more complicated model (eq 3) was justified for only three residues (Leu37, Glu73, and Glu75), while the data for the other residues were more consistent with a simple linear dependence (eq 4). In contrast to the results presented here, a triple mutant of SN stabilized by 3.4 kcal/mol relative to the wild type (44) showed a large fraction of residues with an initial denaturant-independent ΔG_{HX} profile (45). As suggested in our previous report (38) and observed in other studies (46), denaturant-independent ΔG_{HX} profiles appear to be most typical of highly stable proteins with a ΔG^{o}_{unf} of >4-5 kcal/mol (16,18,19).

Extrapolation of the ΔG_{HX} versus urea data to zero denaturant concentration gives ΔG^{o}_{unf}, the standard-state free energy change for unfolding reactions that promote amide exchange. The slope of the denaturant concentration dependence of ΔG_{HX} gives m_{HX}, a parameter related to the change in accessible surface area for the conformational transitions that enable amide proton exchange. The ΔG^{o}_{unf} and m_{HX} data for SN are presented as a function of sequence position in Figure 5. The largest ΔG^{o}_{unf} values measured from the NSHX experiments are on the order of 5.4 kcal/mol, whereas the ΔG^{o}_{unf} obtained from equilibrium denaturation experiments in D_2O at pD 5.2 is 4.0 kcal/mol (32,47). The discrepancy can be explained by the proline effect (22). Prolines have sufficient time to reach their cis–trans equilibrium distribution in conventional denaturation experiments but not in a HX experiment. The HX experiment therefore gives a greater apparent free energy change for complete unfolding, since the protein unfolds to a less populated excited state with a nonequilibrium distribution of cis–trans isomers. This can be corrected using the equation

$$\Delta\Delta G^{o}_{unf} = RT \ln (1 + K_{pro}) \quad (5)$$

where K_{pro} is the equilibrium constant for cis-trans isomerization in the native state (22). There are five trans prolines in native nuclease. Assuming a standard K_{pro} of ¼, the five trans prolines contribute a total of 0.66 kcal/mol at 25 °C. SN also has an additional cis proline at position 117. Here the equilibrium constant favors the cis form (K_{pro}) 4/1) and contributes a $\Delta\Delta G^{o}_{unf}$ of 0.95 kcal/mol. With all prolines identified, the total correction of +1.6 kcal/mol brings the value of 4.0 kcal/mol from equilibrium unfolding experiments (32,47) into very good agreement with the ΔG^{o}_{unf} of 5.4 kcal/mol from HX experiments. The largest m_{HX} values which cluster around 2.5 kcal mol^{-1} M^{-1} are also in excellent agreement with the *m* value of 2.6 obtained from equilibrium denaturation experiments at pH 5.3 (47).

The largest ΔG^{o}_{unf} values from the NSHX experiments cluster to the β-barrel core of the conserved OB-fold motif (Figure 5A). The m_{HX} values follow similar trends (Figure 5B). Table 1 compares the ΔG^{o}_{unf} parameters for SN to those of CspA and LysN, which share the conserved OB-fold motif. In all three proteins, the largest ΔG^{o}_{unf} values are within the OB-fold β-barrel, but as with nuclease, there is a range of stabilities within the β-barrels.

Specifically, strand β1 is less stable than the rest of the β-barrel in SN, which is the case for strand β3 in LysN and strand β5 in CspA. The weakly conserved OB-fold helix in SN, α_{OB}, has a lower average stability than the β-barrel (Table 1). In SN, the first two turns of the α_{OB} helix show no protection but subsequent residues show increased protection that reaches a peak at sequence position 65, near the "hydrophobic plug" residue Val66 and the start of strand β4 (Figure 5A). Of the two α-helices outside of the OB-fold, the C-terminal helix α2 shows the lowest stability of any secondary structure in SN (Figure 5A and Table 1). The first helix outside of the OB-fold, α1 (residues 98–106), is more difficult to interpret. Following strand β5, the segment between residues 97 and 101 is strongly protected but not part of regular secondary structure. In the X-ray structure of SN (PDB entry 1STN), the segment of residues 97–99 folds back to form a short antiparallel β-hairpin interaction with strand β5. The amide proton of residue 100 is hydrogen-bonded to its side chain, and that of residue 101 is protected by burial in the structure since it is not hydrogen-bonded in the X-ray structure. In averaging ΔG°_{unf} for helix α1, we included only those amide protons involved in α-helix hydrogen bonds (residues 102–107) and found that the average stability of helix α1 is comparable or slightly lower than that of the OB-fold helix,α_{OB}.

The stability data from the NSHX studies are mapped on the structures of the three OB-fold proteins in Figure 6. The darkest blue colors correspond to the most stable regions of the structure with the largest ΔG°_{unf} values, which cluster to the structurally conserved OB-fold β-barrels of the three proteins. The light green colors denote the least stable segments that are distributed predominantly in the nonconserved structures, namely, the loops and α-helices. The white segments represent regions where there is no information, typically because exchange was too rapid to quantify.

The ΔG°_{unf} and m_{HX} values from hydrogen exchange are correlated for the three OB-fold proteins (R values of 0.85 for SN, 0.82 for LysN, and 0.54 for CspA), which has been reported for other proteins (43,48). CspA shows only a weak correlation, but this is probably due to the small range of ΔG°_{unf} and m_{HX} values in this protein, where most sites outside of the OB-fold β-barrel exchange too fast to measure (38). Because the parameters are correlated, the structural mapping of m_{HX} values (not shown) is very similar to that for ΔG°_{unf} values (Figure 6). The largest m_{HX} values cluster to the structurally conserved β-barrel. As long as there is no statistical artifact (43), this signifies that the most stable structural elements have the largest structural cooperativity and bury the most solvent accessible area on folding.

To further characterize the exchange properties of the three OB-fold proteins, we collected HX data at basic pHs. Under the conditions of the NSHX studies, all three proteins are in the EX2 regime below pH 7 (not shown). In the EX2 limit, HX rates should theoretically increase by a factor of 10 for every increase in pH unit above pH 4.5 (22). Eventually, the exchange rates reach a plateau in the EX1 limit, and exchange rates no longer depend on stability but on unfolding rates (23,49).

Figure 7 compares $^{1}H–^{15}N$ HSQC spectra of the three OB-fold proteins at neutral and basic pH. As the pH is increased, the rates for the most exchange-susceptible amide protons increase to the point where they are no longer seen in the $^{1}H–^{15}N$ HSQC spectra. These amide protons typically correspond to surface-exposed sites in the three proteins and are colored red in the structural mapping shown in Figure 8. At the next level of protection, amide protons still detected in $^{1}H–^{15}N$ HSQC spectra at pH 11 are colored orange. Within this subset, a fraction of amide protons survive sufficiently long in D_2O to obtain $^{1}H–^{2}H$ exchange rates. The slowly exchanging amide protons are labeled in Figure 7 and are shown on a green (fastest rates) to blue (slowest rates) color ramp in Figure 8. For the least stable protein, CspA, the slowest

exchanging amide protons were identified from saturation transfer experiments at pH 10.8 and 38 °C (23). Exchange rates for SN and LysN were determined in this work by $^{1}H–^{2}H$ isotope exchange experiments. The residues identified as being the most stable to unfolding from the NSHX data in the EX2 limit (Figure 6) correlate with those that exhibit the slowest unfolding rates (k_{open}) in HX experiments conducted in the EX1 exchange limit (Figure 8).

DISCUSSION

Our research on OB-fold proteins (16,17,38,39,50) has been motivated by the hypothesis that information about protein folding intermediates can help shed light on evolutionary relationships between proteins with shared structures, much like protein structures can reveal homology relationships not apparent from protein sequences. Conserved folding pathways have been reported for members of the cytochrome *c* family (51), PDZ domains (52), bacterial immunity proteins (53), and SH3 domains (54). By contrast, different folding mechanisms have been described for proteins within the globin family (55) and for heptameric co-chaperonin protein 10 (56). In the TIM barrel family, folding mechanisms are conserved but there are differences in the structures of intermediates along the folding pathway (57).

Work with OB-fold proteins has concentrated on the structural analysis of partially folded intermediates at equilibrium (58). We initially looked at residual structure under strongly denaturing conditions. An interesting observation to emerge from this work is that the aggregation of CspA, LysN, and SN under acid denaturing conditions is coupled to the propensity of the OB-fold *β*-meander (cyan in Figure 1B) to adopt residual structure in the unfolded states (39,50,59,60). Subsequently, it has been shown that the uncoupling of the *β*-meander from the rest of the CspA structure might have a functional role in nucleic acid binding (61) and that the *β*-meander of CspA can act as a template to fold unrelated sequences in a chimera model of protein structure evolution (62). Partially folded forms of the three proteins with stable tertiary structures have also been investigated. Deletion mutagenesis was used to show that the conserved OB-fold portion of the SN structure can be retained in the absence of two nonconserved α-helices (α1 and α2) that constitute one-third of this single-domain protein (17). Similarly, the OB-fold portion of LysN retains the ability to fold without its nonconserved N-terminal α-helix (16).

NSHX experiments enable a more thorough comparison of partially folded forms and show that the segments of the proteins with the largest stability to unfolding cluster to the conserved OB-fold *β*-barrel (Table 1 and Figure 6). This is not an intrinsic manifestation of *β*-barrels having a larger stability than other types of structures, since individual strands within the *β*-barrel span a range of microscopic stabilities (Table 1). The stability hierarchy shared by the three proteins is evident at the level of the OB-fold supersecondary structure but not when individual structurally analogous sites are compared among the three proteins (Figures 6 and 8). This argues against the hypothesis that specific folding nuclei are needed to form the OB-fold topology (63). Rather, the OB-fold appears to be stabilized by a diffuse network of interactions. Support for this conclusion comes from the unusual global SN suppressor mutants V66L and G88V. The fragment of residues 1–103 of SN with the wild-type sequence has an insufficiently large stability to fold under native conditions but can fold when the V66L and G88V substitutions are incorporated into the sequence. The mutations reinforce the three-layer hydrophobic core of the OB-fold *β*-barrel (17). A second example is provided by the SN fragment Δ131Δ, which is destabilized by 8 kcal/mol compared to the wild type, and is natively unfolded under physiological conditions (27). The fragment regains the native folded structure upon binding of the substrate analogue inhibitor pdTp. These examples highlight that the SN structure can be folded via multiple routes rather than requiring specific nucleation sites.

Taken together, our results for the folding of the three proteins suggest that the OB-fold may represent an ancestral structural motif with the capacity to bind oligonucleotides (7) that was captured and adapted for different functional roles: CspA, a mRNA chaperone; LysN, a tRNA anticodon binding motif; and SN, an enzyme that degrades nucleic acids to nucleotides. Again, it is very difficult to distinguish divergent from convergent evolution. An alternative interpretation for the similar folding hierarchies of the three proteins is that they result from physical constraints on forming the OB-fold structure. An observation we think argues against the latter is that the stability profiles from HX experiments appear to be better conserved among the three distantly related OB-fold proteins CspA, LysN, and SN than between some single-site mutants of SN. The m+ mutants V23A and M26G give HX protection profiles in the absence of denaturants that are nearly uniform as a function of sequence position (32). This has been attributed to a lower propensity of the m+ mutants to form partially folded structures consisting of the OB-motif (32). The substrate analogue inhibitor pdTp in the presence of Ca^{2+} similarly suppresses but does not eliminate the differences in exchange protection between the conserved and nonconserved regions of the SN structure (31). Given that the single-site m+ mutants mentioned above achieve structures similar to that of the wild type, there would not appear to be a strict physical requirement to follow the folding hierarchy observed with the wild-type proteins, at least in vitro. The pronounced effects of the single-site m+ mutants on the stability profile of SN urge caution in concluding that proteins with dissimilar folding pathways lack homology, since even a small change in the sequence can have a dramatic effect on the folding mechanism of otherwise similar proteins.

The functional diversification of OB-fold proteins is exemplified by CspA which presents a hydrophobic surface on its OB-fold β-barrel for mRNA binding (33,44) that is not found in SN or LysN. The nonconserved structural elements unique to SN have a demonstrated functional role in enzymatic activity, with Tyr113 and Tyr115 in the loop between α-helices 1 and 2 forming part of the enzyme's substrate binding site. While a fragment comprising the OB-fold portion of SN can fold in the absence of α-helices 2 and 3, the resulting enzyme is 1000-fold less efficient than the wild type (17). It has been suggested that the flexibility of peripheral structures within an otherwise conserved fold allows for structural diversity, for example, the genesis of new structures through oligomerization (64). There is support for this hypothesis from the OB-fold where the relative independence of the β1–3 meander leads to the apparently conserved aggregation of the acid-denatured states of all three proteins (39,50, 60). Moreover, perturbation of the loop between the nonconserved α-helices 1 and 2 in SN results in a highly stable domain-swapped dimer in which the OB-fold is structurally conserved, and helix α2 swaps from one monomer to the other (65).

Throughout this paper, we have made the distinction between the conserved core parts of the protein structures and the nonconserved auxiliary elements of structure. The distinction is obvious when examples of different structures within the OB-fold superfamily are examined (Figure 1). The results of our folding studies support the distinction based on the conservation of structure. However, is there a physical basis for the distinction between core and peripheral structures that could be predicted if we had fewer examples of OB-fold proteins? Moreover, what accounts for the finer-grained differences between stability profiles, evident even within the conserved β-barrels? In an earlier paper, we noted that the larger stability of the OB-fold β-barrel was consistent with the greater sequence hydrophobicity of this region (16). This conclusion was based on limited NMR studies of deletion mutants of LysN and SN, and NSHX data for only LysN. The more complete NSHX data now available for all three proteins reinforce the agreement with the sequence hydrophobicity profiles (Figure 6 in ref 16). A second parameter that correlates with $\Delta G^{\circ}_{\mathrm{unf}}$ values is the number of long-range contacts (66) for each residue in the structures of the proteins (Figure 9). Correlations between $\Delta G^{\circ}_{\mathrm{unf}}$ and contact density have been noted previously (38,57,67). Exceptions in these trends

are observed, including the underprediction of the ΔG°_{unf} values for α_{OB} and α2 in SN (Figure 9). Overall, however, the contact density captures the stability order of the *β*-strands, and the lowered stability of the accessory structures compared to that of the *β*-barrel core (Figure 9).

The correlation between contact density and stability can be rationalized by considering that the regions of the protein where a change in structure necessitates the disruption of a large number of contacts will be the most difficult to unfold in the reactions that permit amide proton exchange. Similarly, the correlation between microscopic stability and sequence hydrophobicity arises because nonpolar residues are more likely to be buried in the protein cores. The hydrophobicity and contact density parameters are clearly linked, and it may be that a composite of the two may reproduce the experimental ΔG°_{unf} profile better than either parameter alone (57). In the case of SN, there is a wealth of mutagenesis data that also supports a relationship between contact density and stability. The magnitude of the change in stability for mutants in which large hydrophobic residues are substituted with alanine or glycines was found to correlate best with the number of residues within 10 Å of the substituted site (68). Another striking feature of the SN mutants was that they exhibited a bipartite distribution of *m* values with respect to the structure. All of the mutations that increased the *m* value relative to that of the wild type (m+) were in the conserved OB-fold *β*-barrel, while the mutations that decreased the *m* value relative to that of the wild type (m−) were in the nonconserved portions of the structure (68). One way to look at this result is that changes within the conserved core lead to more cooperative denaturation transitions because the *β*-barrel is critical to achieving tertiary structure. By contrast, mutational changes in the remainder of the protein lead to less cooperative denaturation transitions, presumably because the integrity of the conserved *β*-barrel core can to an extent be uncoupled from the nonconserved elements of structure when these are perturbed.

It will be interesting to see if the relationship between contact density and structure conservation holds more generally for other proteins that share the OB-fold motif or indeed extends to proteins in other fold families. If protein structures evolve in stages, the regions with the largest contact densities might correspond to the most structurally conserved regions within fold families. The contact density profile could thus provide a record of the development of protein structure, information that could prove to be useful for elucidating folding mechanisms as well as for protein design applications.

References

1. Stevens RC, Yokoyama S, Wilson IA. Global efforts in structural genomics. Science 2001;294:89–92. [PubMed: 11588249]
2. Chothia C. Proteins. One thousand families for the molecular biologist. Nature 1992;357:543–544. [PubMed: 1608464]
3. Orengo CA, Jones DT, Thornton JM. Protein superfamilies and domain superfolds. Nature 1994;372:631–634. [PubMed: 7990952]
4. Koonin EV, Wolf YI, Karev GP. The structure of the protein universe and genome evolution. Nature 2002;420:218–223. [PubMed: 12432406]
5. Baker D, Sali A. Protein structure prediction and structural genomics. Science 2001;294:93–96. [PubMed: 11588250]
6. Chothia C, Lesk AM. The evolution of protein structures. Cold Spring Harbor Symp Quant Biol 1987;52:399–405. [PubMed: 3454269]
7. Murzin AG. OB(oligonucleotide/oligosaccharide binding)-fold: Common structural and functional solution for non-homologous sequences. EMBO J 1993;12:861–867. [PubMed: 8458342]
8. Gerstein M, Levitt M. A structural census of the current population of protein sequences. Proc Natl Acad Sci USA 1997;94:11911–11916. [PubMed: 9342336]

9. Agrawal V, Kishan RK. Functional evolution of two subtly different (similar) folds. BMC Struct Biol 2001;1:5. [PubMed: 11782293]
10. Arcus V. OB-fold domains: A snapshot of the evolution of sequence, structure and function. Curr Opin Struct Biol 2002;12:794–801. [PubMed: 12504685]
11. Murzin AG, Brenner SE, Hubbard T, Chothia C. SCOP: A structural classification of proteins database for the investigation of sequences and structures. J Mol Biol 1995;247:536–540. [PubMed: 7723011]
12. Murzin AG. How far divergent evolution goes in proteins. Curr Opin Struct Biol 1998;8:380–387. [PubMed: 9666335]
13. Jiang W, Hou Y, Inouye M. CspA, the major cold-shock protein of *Escheichia coli*, is an RNA chaperone. J Biol Chem 1997;272:196–202. [PubMed: 8995247]
14. Commans S, Plateau P, Blanquet S, Dardel F. Solution structure of the anticodon-binding domain of *Escherichia coli* lysyl-tRNA synthetase and studies of its interactions with tRNA(Lys). J Mol Biol 1995;253:100–113. [PubMed: 7473706]
15. Tucker PW, Hazen EEJ, Cotton FA. Staphylococcal nuclease reviewed: A prototypic study in contemporary enzymology. I. Isolation; physical and enzymatic properties. Mol Cell Biochem 1978;22:67–77. [PubMed: 370553]
16. Alexandrescu AT, Jaravine VA, Dames SA, Lamour FP. NMR hydrogen exchange of the OB-fold protein LysN as a function of denaturant: The most conserved elements of structure are the most stable to unfolding. J Mol Biol 1999;289:1041–1054. [PubMed: 10369781]
17. Alexandrescu AT, Gittis AG, Abeygunawardana C, Shortle D. NMR structure of a stable “OB-fold” subdomain isolated from staphylococcal nuclease. J Mol Biol 1995;250:134–143. [PubMed: 7608966]
18. Bai Y, Sosnick TR, Mayne L, Englander SW. Protein folding intermediates: Native-state hydrogen exchange. Science 1995;269:192–197. [PubMed: 7618079]
19. Chamberlain AK, Handel TM, Marqusee S. Detection of rare partially folded molecules in equilibrium with the native conformation of RNaseH. Nat Struct Biol 1996;3:782–787. [PubMed: 8784352]
20. Bai Y, Milne JS, Mayne L, Englander SW. Primary structure effects on peptide group hydrogen exchange. Proteins 1993;17:75–86. [PubMed: 8234246]
21. Zhang, Y-Z. Protein and peptide structure and interactions studied by hydrogen exchange and NMR, PhD Thesis. University of Pennsylvania; Philadelphia: 1995.
22. Bai Y, Milne JS, Mayne L, Englander SW. Protein stability parameters measured by hydrogen exchange. Proteins 1994;20:4–14. [PubMed: 7824522]
23. Rodriguez HM, Robertson AD, Gregoret LM. Native state EX2 and EX1 hydrogen exchange of *Escherichia coli* CspA, a small *β*-sheet protein. Biochemistry 2002;41:2140–2148. [PubMed: 11841204]
24. Flanagan JM, Kataoka M, Fujisawa T, Engelman DM. Mutations can cause large changes in the conformation of a denatured protein. Biochemistry 1993;32:10359–10370. [PubMed: 8399179]
25. Serpersu EH, Shortle D, Mildvan AS. Kinetic and magnetic resonance studies of effects of genetic substitution of a Ca^{2+} -liganding amino acid in staphylococcal nuclease. Biochemistry 1986;25:68–77. [PubMed: 3513826]
26. Shortle D, Meeker AK. Residual structure in large fragments of staphylococcal nuclease: Effects of amino acid substitutions. Biochemistry 1989;28:936–944. [PubMed: 2540825]
27. Alexandrescu AT, Abeygunawardana C, Shortle D. Structure and dynamics of a denatured 131-residue fragment of staphylococcal nuclease: A heteronuclear NMR study. Biochemistry 1994;33:1063–1072. [PubMed: 8110737]
28. Alexandrescu AT, Hinck AP, Markley JL. Coupling between local structure and global stability of a protein: Mutants of staphylococcal nuclease. Biochemistry 1990;29:4516–4525. [PubMed: 2372535]
29. Alexandrescu AT, Snyder DR, Abildgaard F. NMR of hydrogen bonding in cold-shock protein A and an analysis of the influence of crystallographic resolution on comparisons of hydrogen bond lengths. Protein Sci 2001;10:1856–1868. [PubMed: 11514676]
30. Chatterjee S, Jiang W, Emerson SD, Inouye M. The backbone structure of the major cold-shock protein CS7.4 of *Escherichia coli* in solution includes extensive *β*-sheet structure. J Biochem 1993;114:663–669. [PubMed: 8113218]

31. Loh SN, Prehoda KE, Wang J, Markley JL. Hydrogen exchange in unligated and ligated staphylococcal nuclease. Biochemistry 1993;32:11022–11028. [PubMed: 8218167]
32. Wrabl J, Shortle D. A model of the changes in denatured state structure underlying m value effects in staphylococcal nuclease. Nat Struct Biol 1999;6:876–883. [PubMed: 10467101]
33. Feng W, Tejero R, Zimmerman DE, Inouye M, Montelione GT. Solution NMR structure and backbone dynamics of the major cold-shock protein (CspA) from *Escherichia coli*: Evidence for conformational dynamics in the single-stranded RNA-binding site. Biochemistry 1998;37:10881–10896. [PubMed: 9692981]
34. Wang JF, Hinck AP, Loh SN, LeMaster DM, Markley JL. Solution studies of staphylococcal nuclease H124L. 2. ^{1}H, ^{13}C, and ^{15}N chemical shift assignments for the unligated enzyme and analysis of chemical shift changes that accompany formation of the nuclease-thymidine 3′,5′-bisphosphate-calcium ternary complex. Biochemistry 1992;31:921–936. [PubMed: 1731949]
35. Pace CN. Determination and analysis of urea and guanidine hydrochloride denaturation curves. Methods Enzymol 1986;131:266–280. [PubMed: 3773761]
36. Kay LE, Keifer P, Saarinen T. Pure absorption gradient enhanced heteronuclear single quantum correlation spectroscopy with improved sensitivity. J Am Chem Soc 1992;114:10663–10665.
37. Yi Q, Scalley ML, Simons KT, Gladwin ST, Baker D. Characterization of the free energy spectrum of peptostreptococcal protein L. Folding Des 1997;2:271–280.
38. Jaravine VA, Rathgeb-Szabo K, Alexandrescu AT. Microscopic stability of cold shock protein A examined by NMR native state hydrogen exchange as a function of urea and trimethylamine N-oxide. Protein Sci 2000;9:290–301. [PubMed: 10716181]
39. Alexandrescu AT, Rathgeb-Szabo K. An NMR investigation of solution aggregation reactions preceding the misassembly of acid-denatured cold shock protein A into fibrils. J Mol Biol 1999;291:1191–1206. [PubMed: 10518954]
40. Shoemaker, DP.; Garland, CW.; Steinfeld, JI.; Nibler, JW. Experiments in Physical Chemistry. McGraw-Hill; New York: 1981. p. 728-729.
41. Hwang TL, van Zijl PC, Mori S. Accurate quantitation of water-amide proton exchange rates using the phase-modulated CLEAN chemical EXchange (CLEANEX-PM) approach with a Fast-HSQC (FHSQC) detection scheme. J Biomol NMR 1998;11:221–226. [PubMed: 9679296]
42. Anfinsen CB. Principles that govern the folding of protein chains. Science 1973;181:223–230. [PubMed: 4124164]
43. Llinas M, Gillespie B, Dahlquist FW, Marqusee S. The energetics of T4 lysozyme reveal a hierarchy of conformations. Nat Struct Biol 1999;6:1072–1078. [PubMed: 10542101]
44. Chen J, Lu Z, Sakon J, Stites WE. Increasing the thermostability of staphylococcal nuclease: Implications for the origin of protein thermostability. J Mol Biol 2000;303:125–130. [PubMed: 11023780]
45. Wooll JO, Wrabl JO, Hilser VJ. Ensemble modulation as an origin of denaturant-independent hydrogen exchange in proteins. J Mol Biol 2000;301:247–256. [PubMed: 10926507]
46. Chamberlain AK, Marqusee S. Molten globule unfolding monitored by hydrogen exchange in urea. Biochemistry 1998;37:1736–1742. [PubMed: 9492739]
47. Whitten ST, Garcia-Moreno EB. pH dependence of stability of staphylococcal nuclease: Evidence of substantial electrostatic interactions in the denatured state. Biochemistry 2000;39:14292–14304. [PubMed: 11087378]
48. Bollen YJ, Kamphuis MB, van Mierlo CP. The folding energy landscape of apoflavodoxin is rugged: Hydrogen exchange reveals nonproductive misfolded intermediates. Proc Natl Acad Sci USA 2006;103:4095–4100. [PubMed: 16537490]
49. Hvidt A, Nielsen SO. Hydrogen exchange in proteins. Adv Protein Chem 1966;21:287–386. [PubMed: 5333290]
50. Alexandrescu AT, Lamour FP, Jaravine VA. NMR evidence for progressive stabilization of native-like structure upon aggregation of acid-denatured LysN. J Mol Biol 2000;295:239–255. [PubMed: 10623523]
51. Travaglini-Allocatelli C, Gianni S, Brunori M. A common folding mechanism in the cytochrome c family. Trends Biochem Sci 2004;29:535–541. [PubMed: 15450608]

52. Chi CN, Engstrom A, Gianni S, Larsson M, Jemth P. Two conserved residues govern the salt and pH dependencies of the binding reaction of a PDZ domain. J Biol Chem 2006;281:36811–36818. [PubMed: 17018532]
53. Friel CT, Capaldi AP, Radford SE. Structural analysis of the rate-limiting transition states in the folding of Im7 and Im9: Similarities and differences in the folding of homologous proteins. J Mol Biol 2003;326:293–305. [PubMed: 12547210]
54. Korzhnev DM, Neudecker P, Zarrine-Afsar A, Davidson AR, Kay LE. Abp1p and Fyn SH3 domains fold through similar low-populated intermediate states. Biochemistry 2006;45:10183.
55. Nishimura C, Prytulla S, Jane Dyson H, Wright PE. Conservation of folding pathways in evolutionarily distant globin sequences. Nat Struct Biol 2000;7:679–686. [PubMed: 10932254]
56. Luke K, Perham M, Wittung-Stafshede P. Kinetic folding and assembly mechanisms differ for two homologous heptamers. J Mol Biol 2006;363:729–742. [PubMed: 16979655]
57. Gu Z, Zitzewitz JA, Matthews CR. Mapping the Structure of Folding Cores in TIM Barrel Proteins by Hydrogen Exchange Mass Spectrometry: The Roles of Motif and Sequence for the Indole-3-glycerol Phosphate Synthase from *Sulfolobus solfataricus*. J Mol Biol 2007;368:582–594. [PubMed: 17359995]
58. Wang Y, Alexandrescu AT, Shortle D. Initial studies of the equilibrium folding pathway of staphylococcal nuclease. Philos Trans R Soc London Ser B 1995;348:27–34. [PubMed: 7770483]
59. Wang Y, Shortle D. The equilibrium folding pathway of staphylococcal nuclease: Identification of the most stable chain-chain interactions by NMR and CD spectroscopy. Biochemistry 1995;34:15895–15905. [PubMed: 8519746]
60. Ye K, Wang J. Self-association reaction of denatured staphylococcal nuclease fragments characterized by heteronuclear NMR. J Mol Biol 2001;307:309–322. [PubMed: 11243822]
61. Max KE, Zeeb M, Bienert R, Balbach J, Heinemann U. Common mode of DNA binding to cold shock domains. Crystal structure of hexathymidine bound to the domain-swapped form of a major cold shock protein from *Bacillus caldolyticus*. FEBS J 2007;274:1265–1279. [PubMed: 17266726]
62. Reichmann L, Winter G. Novel folded protein domains generated by combinatorial shuffling of polypeptide segments. Proc Natl Acad Sci USA 2000;97:10068–10073. [PubMed: 10954734]
63. Mirny LA, Shakhnovich EI. Universally conserved positions in protein folds: Reading evolutionary signals about stability, folding kinetics and function. J Mol Biol 1999;291:177–196. [PubMed: 10438614]
64. Andreeva A, Murzin AG. Evolution of protein fold in the presence of functional constraints. Curr Opin Struct Biol 2006;16:399–408. [PubMed: 16650981]
65. Green SM, Gittis AG, Meeker AK, Lattman EE. One-step evolution of a dimer from a monomeric protein. Nat Struct Biol 1995;2:746–751. [PubMed: 7552745]
66. Sobolev V, Sorokine A, Prilusky J, Abola EE, Edelman M. Automated analysis of interatomic contacts in proteins. Bioinformatics 1999;15:327–332. [PubMed: 10320401]
67. Bahar I, Wallqvist A, Covell DG, Jernigan RL. Correlation between native-state hydrogen exchange and cooperative residue fluctuations from a simple model. Biochemistry 1998;37:1067–1075. [PubMed: 9454598]
68. Shortle D, Stites WE, Meeker AK. Contributions of the large hydrophobic amino acids to the stability of staphylococcal nuclease. Biochemistry 1990;29:8033–8041. [PubMed: 2261461]
69. Lo Conte L, Brenner SE, Hubbard TJ, Chothia C, Murzin AG. SCOP database in 2002: Refinements accommodate structural genomics. Nucleic Acids Res 2002;30:264–267. [PubMed: 11752311]
70. Carra JH, Privalov PL. Thermodynamics of denaturation of staphylococcal nuclease mutants: An intermediate state in protein folding. FASEB J 1996;10:67–74. [PubMed: 8566550]

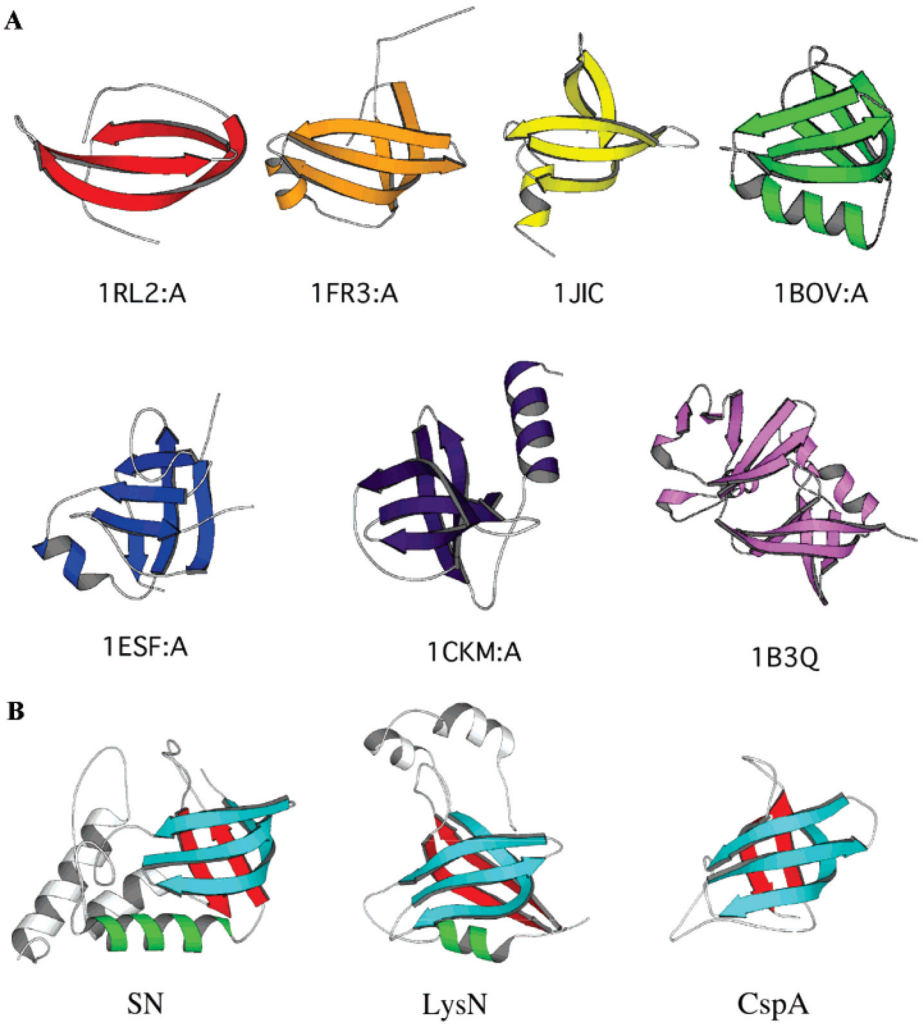

Figure 1.

Structural variability in OB-fold proteins. (A) Proteins currently assigned to the OB-fold in the SCOP database (69) range from a three-stranded *β*-meander (PDB entry 1RL2) to a 10-stranded *β*-sheet thought to correspond to a domain-swapped duplication of the motif (PDB entry 1B3Q). (B) Three OB-fold proteins used as a model system for comparative protein folding studies in our lab (16,17,38,39,50). The structurally conserved core of these proteins consists of a *β*-meander (blue) and a *β*-hairpin (red) that come together to form a five-stranded *β*-barrel. The *β*-barrel is closed by an antiparallel *β*1–*β*4 interaction and a distorted parallel *β*3–*β*5 pairing. In the original definition of the OB-fold (7), an α-helix (green) capped the bottom of the *β*-barrel. When present, this α-helix is structurally poorly conserved, and many proteins currently classified in the OB-fold group such as CspA lack it entirely (69). Nonconserved elements of structure outside the OB-fold are left uncolored.

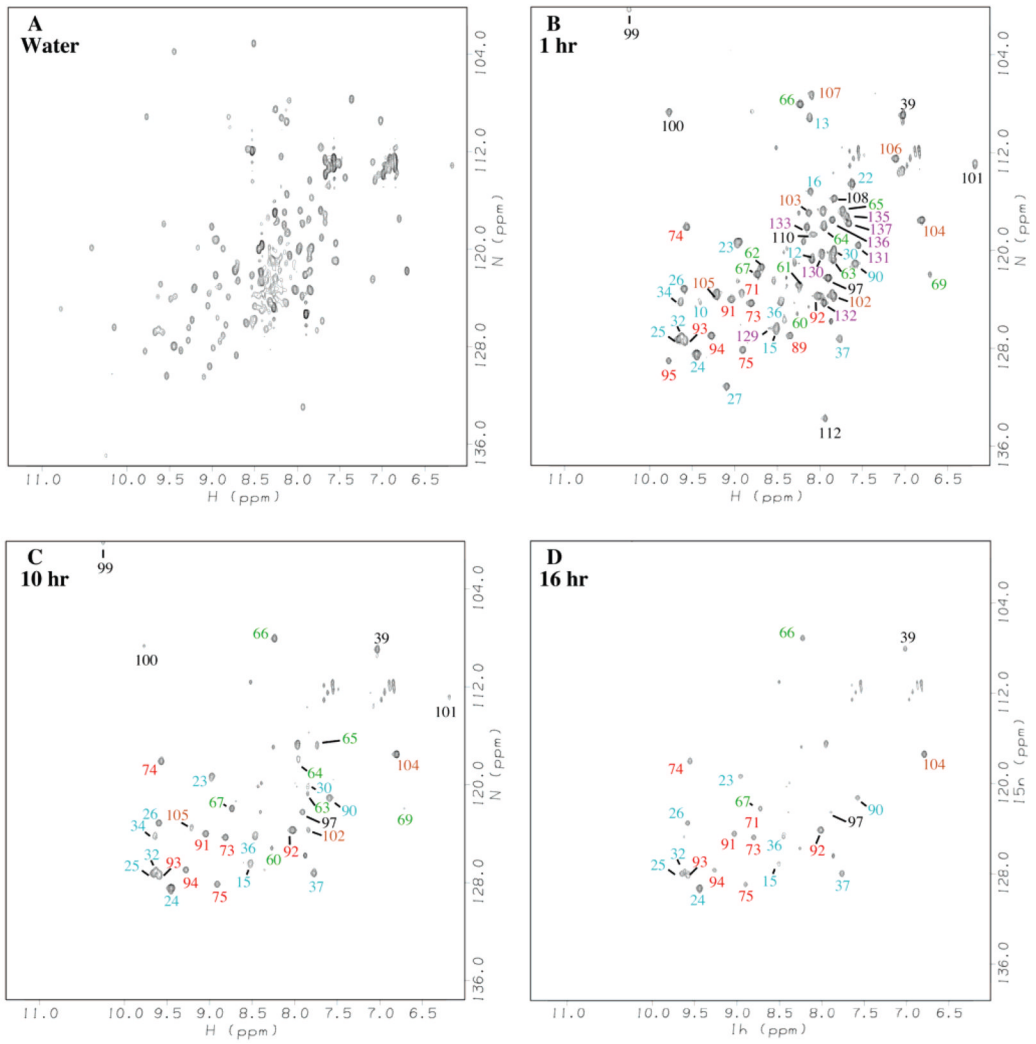

Figure 2.

Representative $^{1}H–^{15}N$ HSQC spectra used to monitor HX in the absence of urea: (A) spectrum in H_2O and spectra after exchange in D_2O for 1 (B), 10 (C), and 16 h (D). The SN sample was in 20 mM sodium acetate buffer (pD 5.3). Signals from protected amide protons in panels B–D are labeled by sequence position and colored according to secondary structure: β1–3 meander, cyan; β4–5 hairpin, red; helix α 1, green; helix α2, brown; helix α3, violet; and other, black. Cross-peaks that could not be characterized due to overlap or missing assignments are unlabeled. Residues Thr22, Val39, Ala69, Glu101, and Ala109 are protected in spite of not being involved in hydrogen bonds in the X-ray structure (PDB entry 1SNT).

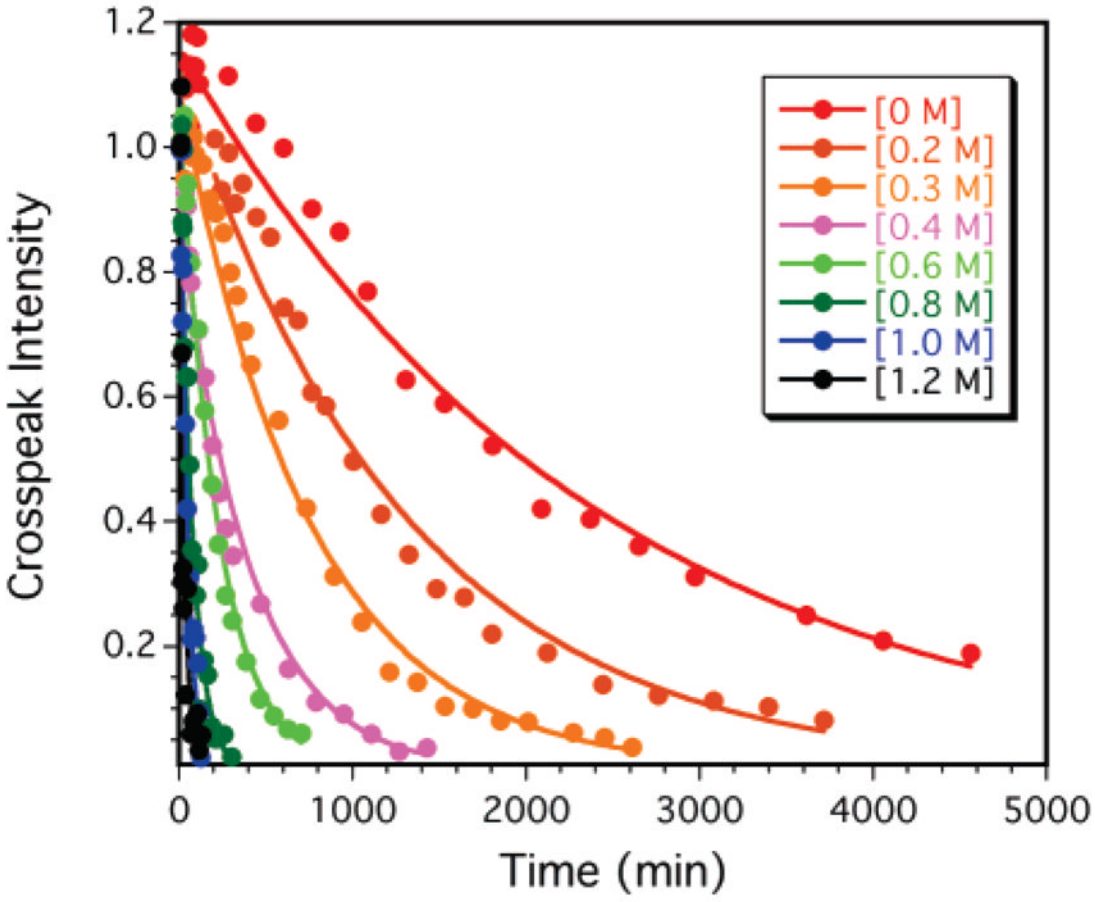

Figure 3.
Exponential decays of $^{1}H–^{15}N$ cross-peak intensities due to exchange at different urea concentrations. Data are shown for the representative residue, Lys24.

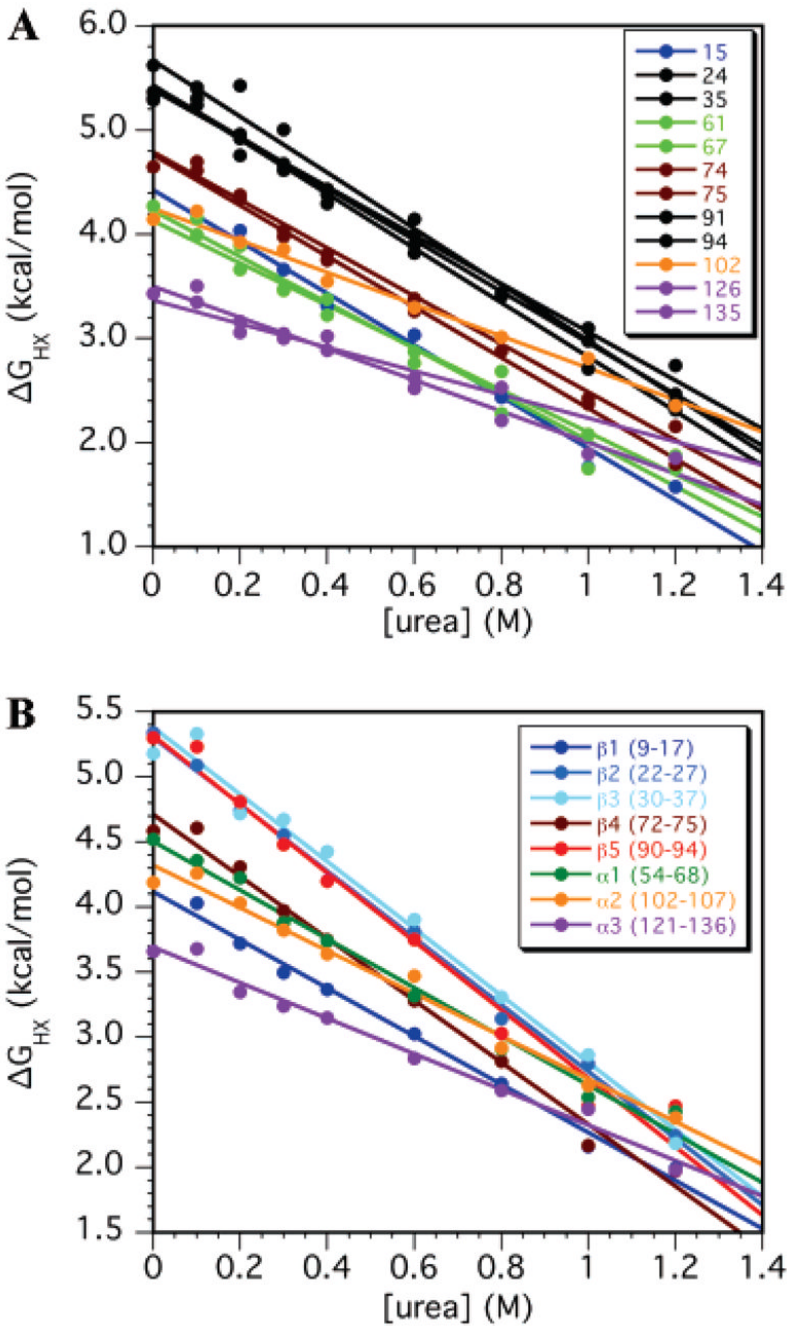

Figure 4.
HX isotherms for (A) individual residues and (B) averages over the indicated secondary structures.

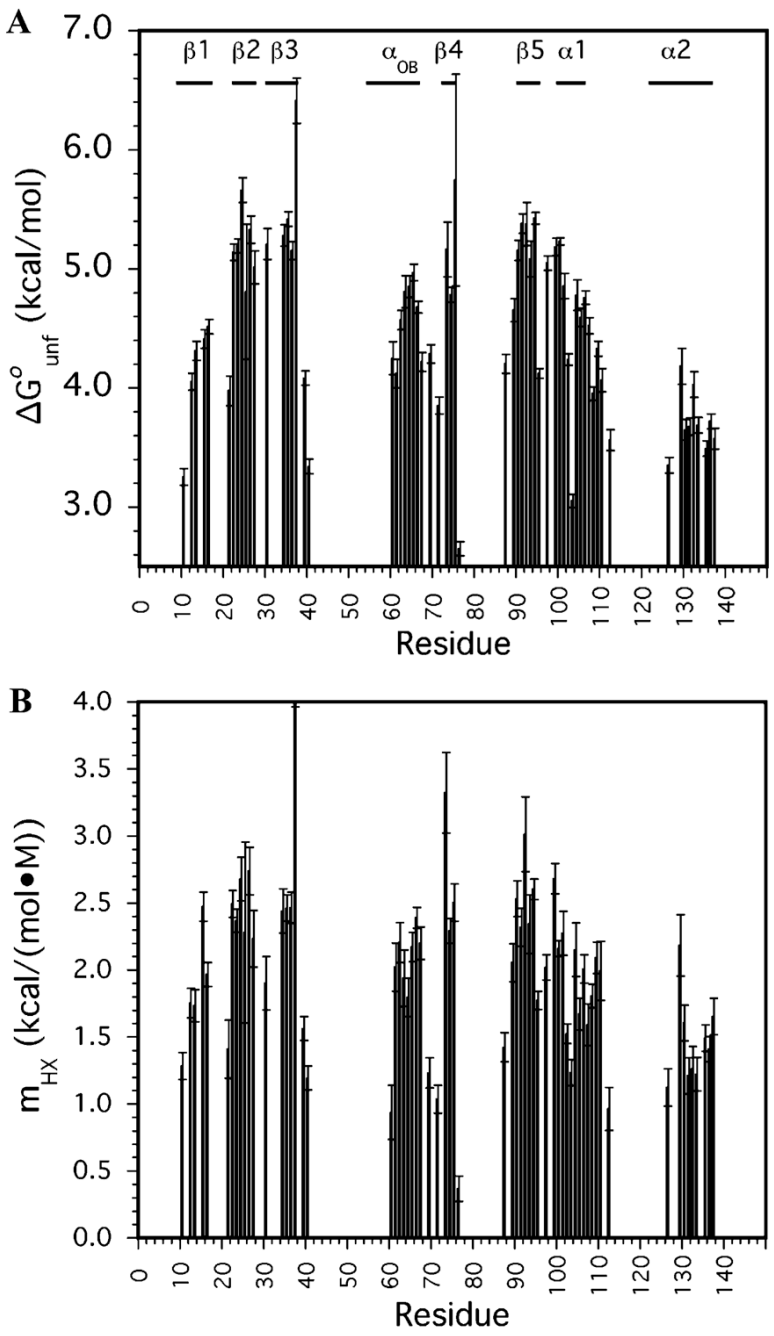

Figure 5.

Thermodynamic parameters from NSHX experiments with SN. (A) $\Delta G^{\circ}_{\mathrm{unf}}$ the standard-state free energy of unfolding (18). (B) m_{HX}, the slope of the ΔG_{HX} dependence on denaturantconcentration, which is related to the cooperativity (70) or the change in accessible surface area accompanying unfolding (68). Secondary structure boundaries are indicated at the top of the figure.

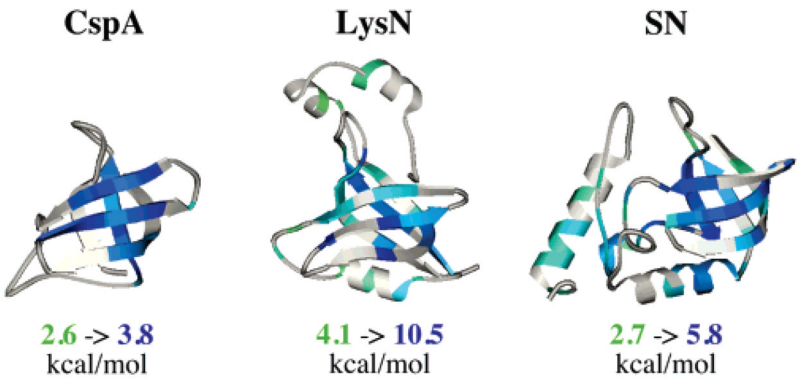

Figure 6.

Structural mapping of ΔG°_{unf} values. SN data are from this work, and those for CspA (38) and LysN (16) were previously published. ΔG°_{unf} ranges are given below each structure. The most stable regions of the structures are colored dark blue and the least stable regions bright green. Uncolored regions indicate no information is available; most of these sites exchange too fast to measure.

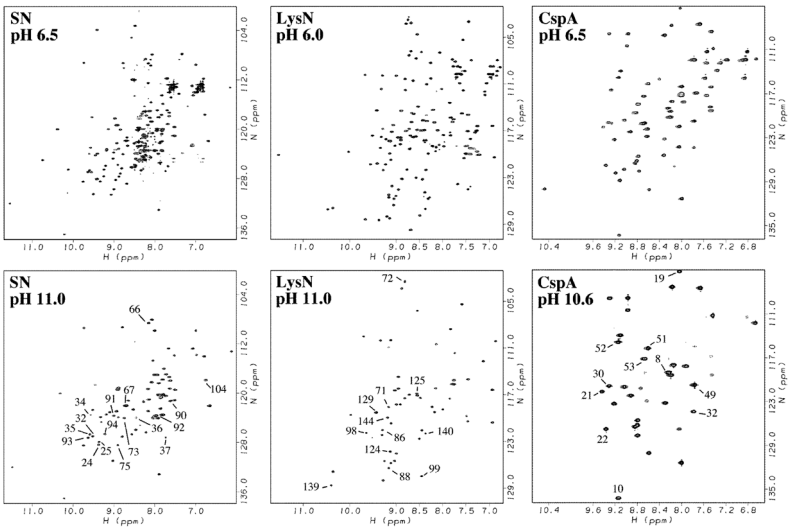

Figure 7.

Comparisons of $^{1}H–^{15}N$ HSQC spectra for SN, LysN, and CspA at neutral and basic pHs. The spectra were acquired at 25 °C. Under EX2 conditions, HX rates increase 10-fold for every pH unit, causing correlations from the most exchange-susceptible sites to be lost at basic pHs (bottom panels). Within the subset of correlations that persist, the cross-peaks that are labeled in the figure correspond to the slowest exchangers, identified for CspA from NMR saturation transfer experiments at pH 10.8 (23) and for LysN and SN from $^{1}H–^{2}H$ isotope exchange experiments at pH 10.2 (this work).

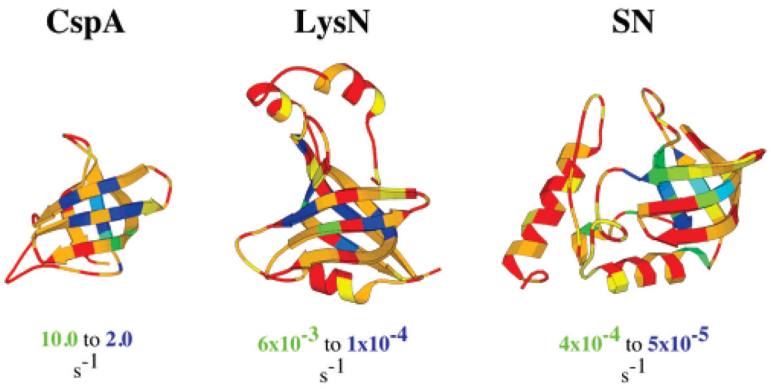

Figure 8.

EX1 exchange data at basic pH mapped onto the structures of the three OB-fold proteins. The slowest exchanging protons were determined from isotope exchange experiments at pH 10.2 for LysN (15 °C) and SN (23 °C) and from NMR saturation transfer experiments at pH 10.8 and 38 °C for CspA (23). The slowest exchangers are shown on a color ramp similar to that of Figure 6 where green indicates faster exchange and blue corresponds to slower rates. Additional colors are as follows: red, observed at neutral but not basic pH; orange, observed above pH 10 but exchange is too fast to determine rates from $^{1}H–^{2}H$ isotope exchange experiments; and yellow, not determined due to overlap or missing assignments.

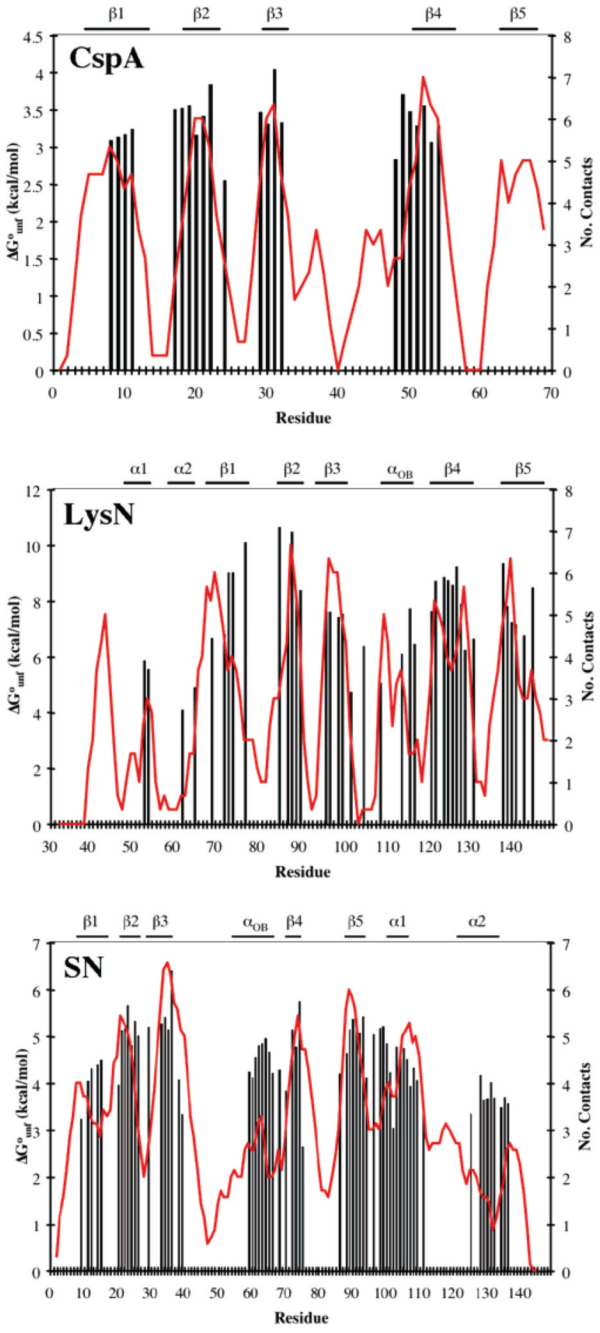

Figure 9.

Comparison of G^{o}_{unf} values from hydrogen exchange (bar graphs) with inter-residue contacts (red lines) calculated with CMA (66). The structures of each of the three OB-fold proteins (PDB entries 1MJC, 1KRS, and 1STN) were used as input for the calculations. Only contacts between residues separated by more than five positions in the sequence were considered in the analysis. Contact data were averaged over a window of three residues for CspA and LysN and a window of seven residues for SN.

Table 1

ΔG^{o}_{unf} Values (kilocalories per mole), Averaged over Secondary Structure Elements and Subdomains in the Three OB-Fold Proteins (SN, LysN, and CspA)[a]

structure element[b]	SN	LysN	CspA
*β*1	4.1 ± 0.5	8.3 ± 1.5	3.2 ± 0.1
*β*2	5.2 ± 0.3	9.1 ± 1.4	3.5 ± 0.2
*β*3	5.5 ± 0.5	7.6 ± 0.1	3.6 ± 0.4
*β*4	5.2 ± 0.5	8.1 ± 1.0	3.3 ± 0.2
*β*5	5.1 ± 0.5	7.8 ± 1.0	1.7 ± 0.6[c]
α_{OB}	4.6 ± 0.3	6.4 ± 1.1	NP[d]
α1	4.3 ± 0.6	5.7 ± 0.2	NP[d]
α2	3.7 ± 0.2	4.5 ± 0.6	NP[d]
β-barrel	5.0 ± 0.6	8.2 ± 1.1	3.0 ± 0.8
α-helices	4.2 ± 0.5	5.7 ± 1.1	NP[d]
all except *β*-barrel	4.2 ± 0.6	5.7 ± 1.0	2.8 ± 0.7

[a] The values for SN are from the study presented here, while those for CspA and LysN are from previously published work (16,38).

[b] Sequence positions for elements of regular secondary structure are defined as follows: SN (*β*1, 9–19; *β*2, 22–27; *β*3, 29–37; α_{OB}, 54–67; *β*4, 72–75; *β*5, 90–95; α1, 102–107; α2, 121–135), LysN (α1, 46–54; α2, 58–64; *β*1, 67–79; *β*2, 84–90; *β*3, 93–100; α_{OB}, 108–116; *β*4, 120–130; *β*5, 137–147), and CspA (*β*1, 5–13; *β*2, 18–23; *β*3, 30–33; *β*4, 50–56; *β*5, 63–69). The first 30 residues of the LysS lysyl-tRNA synthetase are missing in the LysN fragment (14). For consistency with previously published numbering schemes, we designate the first residue of LysN as Ala30 (14,16).

[c] For CspA strand *β*5, and for residues outside of the *β*-barrel, the numbers cited are from the dependence of HX on the stabilizer trimethylamine *N*-oxide (TMAO), because the amide protons in question exchanged too fast to measure in the presence of urea (38). All other CspA values are from urea experiments.

[d] Not present.